Tunable Rectification of Diffusion-Wave Fields by Spatiotemporal Metamaterials

Jiaxin Li,[1,*] Zhanxiang Zhang,[2,*] Guoqiang Xu,[1] Haoran Sun,[2] Lizhou Dai,[2] Tianlong Li,[2,†] and Cheng-Wei Qiu[1,‡]
[1]Department of Electrical and Computer Engineering, National University of Singapore, Singapore 117583, Singapore
[2]State Key Laboratory of Robotics and System, Harbin Institute of Technology, Harbin 150001, China

(Received 5 June 2022; accepted 25 October 2022; published 16 December 2022)

The diffusion process is the basis of many branches of science and engineering, and generally obeys reciprocity between two ports of a linear time-invariant medium. Recent research on classical wave dynamics has explored the spatiotemporal modulation to exhibit preferred directions in photons and plasmons. Here we report a distinct rectification effect on diffusion-wave fields by modulating the conductivity and observe nonreciprocal transport of charges. We experimentally create a spatiotemporal diffusion metamaterial, in which a mode transition to zero frequency is realized. A direct current component thereby emerges, showcasing a biased effect on the charge diffusion when the incident fundamental frequency is a multiple of the system modulation frequency. These results may find applications spanning a plethora of diffusive fields in general.

DOI: 10.1103/PhysRevLett.129.256601

For some time, several diffusion-related periodic phenomena have become unified under the global mathematical label of diffusion-wave field [1,2], mainly including the categories of charge- carrier-density waves, thermal waves [3,4], chemical waves [5], etc. Generally, such propagation in linear, nonbiased, and time-invariant materials obeys reciprocity [6,7], which means the field transport is symmetric in opposite directions. The recent studies of nonreciprocity [8] induced by spatiotemporal modulation in electromagnetic [9–11], acoustic [12–14], and elastic [15,16] metamaterials have revealed potential for developing asymmetric transport and flexible manipulation, exhibiting advantages in more diverse signal and energy transmission. However, realizing nonreciprocal diffusion-wave field propagation is intrinsically elusive, due to the intrinsic reciprocity and unclear symmetry-breaking mechanism endorsed by diffusive nature. Though several spatiotemporal diffusion systems [17,18] have also exhibited asymmetry, the nonreciprocal mode transition subject to periodic excitation has not been explored, in an analogy to photonic transitions induced by refractive index modulation [19–21]. As such, the successful realization of spatiotemporal diffusion-wave metamaterials simultaneously implies the fundamental significance of nonreciprocity in diffusion-related periodic transports, and the industrial benefits in applications with alternating current (ac), fluctuating temperature, varying particle concentration, etc.

As a typical characteristic of nonreciprocal transfer, some drag effects of physical fields have been observed, such as Fizeau drag of light [22,23], plasmon polaritons [24,25], and thermal waves [26], meaning that the waves travel at different speeds along and against the moving or modulation direction of media. Here we report another kind of drag effect on diffusion waves. Thanks to the mode transitions [14,19–21] to zero frequency caused by a conductivity modulation synchronized with the periodic excitation, a dc component emerges and "drags" the transmission potential Φ_T away from the previous average of the input potential Φ_I, as shown in Figs. 1(a) and 1(b). A fundamental framework is established to analyze the system, thus deriving the dispersion relation, harmonic generation, transmission spectrum, and nonreciprocal effects. A confirmatory experiment is conducted to verify the conversion from ac to dc and nonreciprocal transport of charge diffusion waves. This discovery might reduce the dependence on inversion-symmetry-broken materials [27] (such as the semiconductor p–n junction) in direction-dependent charge transport, and further realize ac-dc converters, rectifiers, diodes, and isolators with isotropic and linear materials. Besides, this mechanism is applicable to a wide range of diffusion phenomena that obeys Fick's law, including charge diffusion, mass transport, and heat transfer.

The diffusion processes are mainly governed by Fick's diffusion equation, which describes physical quantities (e.g., energy or discrete particles) driven by potential gradients as driving forces. Its most general form is $\partial(c\Phi)/\partial t = \nabla\cdot(\sigma\nabla\Phi)$, where Φ is the potential field, t is time, σ and c are the conductivity and capacity of the medium, respectively. Figures 1(a) and 1(b) depict the general representation of a spatiotemporally modulated medium (length L), with the diffusion waves traveling towards the forward (left) and backward (right) directions. An oscillating potential boundary $\Phi_I(t)$ with frequency ω_0 is applied at one end to imitate an incident wave, while zero-flux boundary condition is taken at the other to observe a transmission potential $\Phi_T(t)$. For the

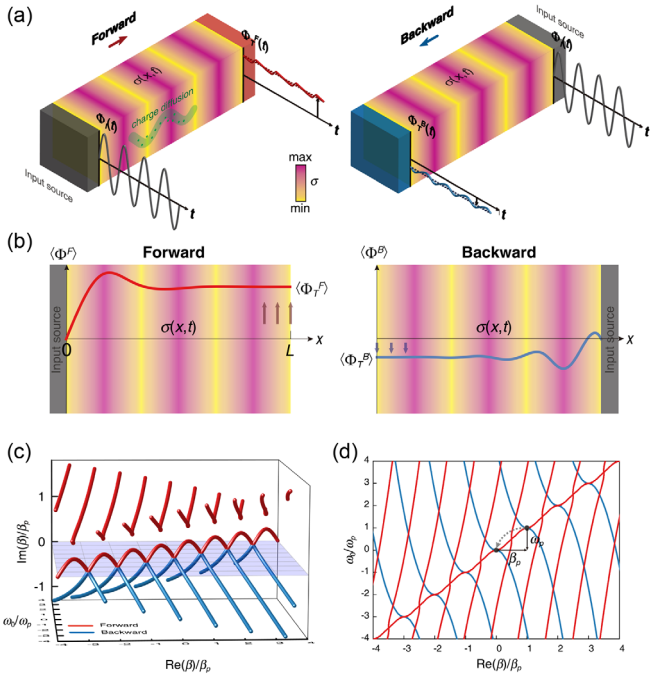

FIG. 1. Conceptual representation and dispersion relation of diffusion waves through a spatiotemporally modulated medium. (a) Nonreciprocal forward and backward transmission (Φ_T^F and Φ_T^B) of a diffusion wave (excited by a sinusoidal input potential Φ_I) can be induced, using a medium whose conductivity $\sigma(x,t)$ is spatiotemporally modulated. For some cases where the excitation frequency is a multiple of the modulation frequency, there exists a zero-frequency harmonic, or dc component, dragging the average of the transmission potential Φ_T away from that of Φ_I. (b) The time-averaged potential distribution $\langle\Phi^F\rangle$ and $\langle\Phi^B\rangle$ along x at the quasisteady state. (c) Dispersion diagrams for the spatiotemporally modulated medium. Red and blue curves represent, respectively, the excited forward and backward space-time modes within a range of incident frequency ω_0. (d) The projection of the dispersion diagram on Re(β)-ω_0 plane. The arrow indicates the mode transition accompanied by the frequency shift ω_p and wave number shift β_p.

one-dimensional (1D) spatiotemporal medium, the governing diffusion equation becomes

$$c_0\frac{\partial\Phi(x,t)}{\partial t}=\frac{\partial}{\partial x}\left[\sigma(x,t)\frac{\partial\Phi(x,t)}{\partial x}\right], \tag{1}$$

where the capacity c_0 is a constant, and the conductivity is modulated as a traveling wave of both space x and time t: $\sigma(x,t)=\sigma(\beta_p x-\omega_p t)$, where β_p and ω_p are the spatial and temporal frequencies of the modulation wave, respectively. Applying Floquet-Bloch theorem, the potential field $\Phi(x,t)$ inside the metamaterial should be a superposition of the eigenfunctions

$$\Phi(x,t)=e^{i(\beta x-\omega_0 t)}\sum_m F_m e^{im(\beta_p x-\omega_p t)} \tag{2}$$

where β is the wave number of the pseudo diffusion plane wave calculated based on the fundamental frequency ω_0 excited by the oscillating source, and F_m ($m=0,\pm1,\pm2,\ldots$) are the Fourier coefficients of Floquet-Bloch harmonics. Taking the framework of charge transport as an example, we obtain the dispersion relation (Supplemental Material 1-2 [28]) of the medium with a sinusoidal modulated conductivity $\sigma=\sigma_0[1+\Delta_\sigma\cos(\beta_p x-\omega_p t)]$, where $\sigma_0=1$ S m, $\Delta_\sigma=0.9$, $\beta_p=2\pi$ m^{-1}, and $\omega_p=4\pi$ s^{-1}. Other parameters are set as $c_0=1$ F m^{-1} and $L=1$ m. We truncate the Fourier expansions to the tenth order to achieve a precise solution of the dispersion relation presented by the 3D curves in Fig. 1(c). Different from electromagnetic wave propagation [29,30] in dielectrics and free space, whose dispersion diagram is mainly plotted with pure real wavenumbers, Fig. 1(c) shows that here almost all the wave numbers β are complex with nonzero imaginary parts, indicating the spatial attenuation of the diffusion system. Several modes $(\beta,\omega_0)=(n\beta_p,n\omega_p)$ (n is an integer) are located on Im(β) = 0 plane, which are also the intersections of the forward and backward space-time harmonics. The dispersion diagram exhibits periodicity only with respect to Re(β) and ω_0, so we plot its projection on Re(β) $-\omega_0$ plane in Fig. 1(d). A repeated cell pattern appears along a straight line whose slope equals the phase velocity of the pump modulation [the slope is equal to 1 in Fig. 1(d) as a result of the normalization of coordinates]. The frequency shift ω_p and wave number shift β_p induced by the spatiotemporal modulation can be easily seen, which can be viewed as a counterpart of mode transitions [14,19–21] in modulated diffusion systems. Especially when the "incident" frequency $\omega_0=n_0\omega_p$ (n_0 is an integer), the mode transitions will cause a zero-frequency component, leading to a biased effect. In addition, nonreciprocity from the breaking of time-reversal symmetry is observed, presented as the asymmetric tilted dispersion curves and different propagating speeds along forward and backward directions. This asymmetry is positively related to the modulation depth Δ_σ (see Fig. S1 [28]). Note that nonreciprocity cannot be generated by a pure time modulation ($\beta_p=0$) or a pure space modulation ($\omega_p=0$). See the discussion of these two special cases in Supplemental Material 3 and Figs. S2–S3 [28].

To specifically demonstrate the transmission properties of the diffusion waves, we plot the transmission potential for different frequencies of the input potential Φ_I in Fig. 2. The material parameters for the results in Fig. 2 are the same as in Fig. 1(c). The boundary condition at the input end is set to be $\Phi_I=A_0\cos(\varphi-\omega_0 t)$, where $A_0=1$ V, $\varphi=\pi/2$, and $\omega_0/\omega_p=0.2$, 1, 1.1, and 2. The analytical results (Supplemental Material 4 [28]) fit well with finite-element simulations using COMSOL Multiphysics®, verifying the accuracy of our analytical solutions. As shown in the cases $\omega_0=\omega_p$ and $\omega_0=2\omega_p$, the transmission potential is dragged, for the average of potential over time $\langle\Phi_T\rangle$

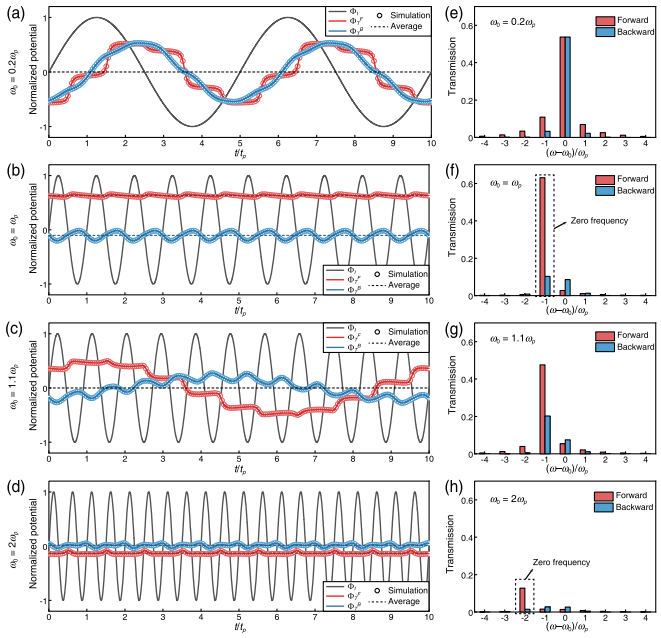

FIG. 2. Transmission through a spatiotemporally modulated medium. (a)–(d) Forward and backward transmission potentials corresponding to different frequencies of the input potential Φ_I: $\omega_0 = 0.2\omega_p$ (a), $\omega_0 = \omega_p$ (b), $\omega_0 = 1.1\omega_p$ (c), and $\omega_0 = 2\omega_p$ (d). In the cases $\omega_0 = \omega_p$ and $2\omega_p$, a potential drag occurs because the average of Φ_T over time is nonzero, while in the cases $\omega_0 = 0.2\omega_p$ and $1.1\omega_p$, the time-averaged potential remains 0. Lines are analytical results, scatter points are simulated results, and dashed lines are analytical solutions of the time-averaged potential. (e)–(h) Analytical transmission spectrum corresponding to (a)–(d). Higher order harmonics (the $\pm 1^{\text{st}}, \pm 2^{\text{nd}}, \ldots$ orders) appear around the fundamental frequency ω_0, and the zero-frequency harmonic is generated at the -1^{st} order when $\omega_0 = \omega_p$ (at the -2^{nd} order when $\omega_0 = 2\omega_p$).

is nonzero. We therefore refer to the cases $\omega_0 = n_0\omega_p$ as *coupled* case for brevity. On the contrary, for $\omega_0 \neq n_0\omega_p$, which is called *uncoupled* case, the time-averaged potential $\langle\Phi_T\rangle$ remains 0, as confirmed in the cases $\omega_0 = 0.2\omega_p$ and $\omega_0 = 1.1\omega_p$. We give the analytical transmission spectrum in Figs. 2(e)–2(h), corresponding to the four cases in Figs. 2(a)–2(d). It can be seen that under spatiotemporal modulation, higher order harmonics (the $\pm 1^{\text{st}}, \pm 2^{\text{nd}}, \ldots$ orders) appear around the fundamental frequency ω_0, thus modulating the waveform of Φ_T. Specially, when the incident frequency ω_0 is close to the modulation frequency ω_p, there exists a low-frequency harmonic $\omega_{\text{beat}} = \omega_0 - \omega_p$, just like beats produced by the superposition of two harmonic oscillations with nearly equal frequencies [31]. As the example $\omega_0 = 1.1\omega_p$ shown in Fig. 2(c), the period of Φ_T turns to be 10 times the modulation temporal period. Furthermore, as $\omega_0 \to \omega_p$, the period of beat approaches infinity. According to Eq. (2), when $\omega_0 = n_0\omega_p$, the $(-n_0)$ order of transmission spectrum is zero frequency and corresponds to the time-averaged potential $\langle\Phi_T\rangle$.

The difference in the waveform as well as the transmission spectrum between the forward and backward directions reflects the nonreciprocal effect of spatiotemporal modulation on the diffusion waves. A feature is that the incident wave seems to be more efficiently converted to higher-order harmonics in the forward direction, originating from the fact that the dispersion curves representing the forward harmonics are closer to each other than the backward ones. As an exception, when Φ_I remains constant ($\omega_0 = 0$), the potential distribution along the entire transmission path will be $\Phi(x,t) = \Phi_I$, implying that the modulation does not make any difference in forward and backward directions. This is identical with the view of previous works [17,18] that two material parameters must be modulated simultaneously to obtain nonreciprocity in diffusive systems under constant boundary conditions. It should be added that our theory also applies to thermal waves. If the input temperature is oscillating around a reference temperature T_{ref}, there will be a temperature offset with respect to T_{ref} at the output end for the coupled case, based on the principle of superimposition.

In the following, we discuss the drag effect on the dc component of various modulation parameters in coupled cases. The analytical results of $\langle\Phi_T\rangle$ in Fig. 3 illustrate the dependence of the potential drag on the modulation depth Δ_σ, modulation phase velocity v_p (defined as $v_p = \omega_p/\beta_p$, where β_p is taken to be constant and ω_p is varying in order to adjust v_p), and the initial phase φ of the input potential. The input frequency is taken as $\omega_0 = \omega_p$, and other parameter settings in Fig. 3 are the same as in Fig. 2, except the argument of concern. From Fig. 3(a), we see that

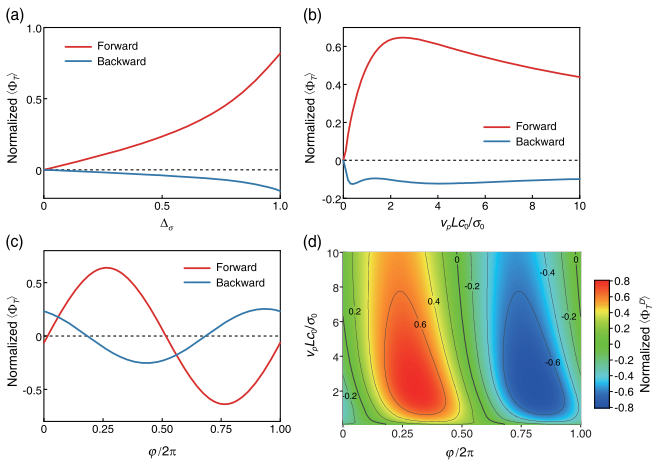

FIG. 3. Influence of modulation parameters on the time-averaged potential and nonreciprocity. Dependence of transmission potential drag on the modulation depth Δ_σ (a), modulation phase velocity v_p (b), and initial phase φ (c). (d) Degree of nonreciprocity (defined as $\langle\Phi_T^D\rangle = \langle\Phi_T^F\rangle - \langle\Phi_T^B\rangle$) for various combinations of v_p and φ.

as the increase of the modulation depth Δ_σ, the potential drag characterized by $\langle\Phi_T\rangle$ becomes larger. The effect of the modulation phase speed v_p is depicted in Fig. 3(b), where the absolute value of $\langle\Phi_T\rangle$ increases as v_p increases from 0 and decreases from ∞. Both $\langle\Phi_T^F\rangle$ and $\langle\Phi_T^B\rangle$ approach 0 when $v_p \to 0$ and ∞, so nonreciprocity will disappear under these circumstances. The dependence of $\langle\Phi_T\rangle$ on the initial phase φ is shown by the sinusoidal curve in Fig. 3(c). [This sinusoidal function can be reflected from Eq. (S30) in the Supplemental Material [28].] The drag effect appearing in the transmission potential can be either positive or negative under the modulation of φ, meaning that it can even oppose the modulation phase speed. It can be seen that the value range of $\langle\Phi_T^F\rangle$ is larger than that of $\langle\Phi_T^B\rangle$, as a result of the stronger transitions in the forward direction. We define the difference $\langle\Phi_T^D\rangle = \langle\Phi_T^F\rangle - \langle\Phi_T^B\rangle$ to characterize the degree of nonreciprocity. The values of $\langle\Phi_T^D\rangle$ for various combination of v_p and φ are summarized in Fig. 3(d), revealing the controllable nonreciprocity of the spatiotemporal metamaterial. The optimal combination of v_p and φ with maximum nonreciprocity can be found, while the contour line "0" indicates that some combinations of v_p and φ can restore reciprocity of the zero-frequency component.

We then construct an equivalent circuit of 1D metamaterial with spatiotemporally modulated conductivity and demonstrate the aforesaid phenomenon experimentally (see Fig. 4). The circuit in Fig. 4(a) is a lumped parameter model of electric charge diffusion, corresponding to the continuum model in Fig. 1. The governing equation of the circuit can be derived analytically using the Kirchhoff laws, which can be homogenized spatially and equivalent to the differential diffusion equation in Eq. (1) when a large number of components are adopted [18]. Here we use 10 time-varying resistors alternated by 9 fixed capacitors, forming a spatial variation of conductivity along the direction of propagation. The experimental platform is illustrated in Fig. 4(b), where the potentiometers are driven by stepper motors controlled by a microcontroller unit. The resistance of each potentiometer can be adjusted by rotating its spinner handle connected to the shaft of a motor, so the reciprocating rotation of the motor will change the resistance periodically. The resistance of each resistor satisfies $R_i = R_{\min} + \Delta R\,\Pi(\theta_i - \omega_p t)$, where $R_{\min} = 100\,\Omega$, $\Delta R = 2100\ \Omega$, $\Pi(\cdot)$ represents the normalized square dimensionless function, the initial phase $\theta_i = 2\pi(i-1)/10$ and $i = 1, 2, \ldots, 10$. In our experimental setup, the fixed capacitance $C_0 = 235\ \mu\text{F}$, and the modulation period $t_p = 2\pi/\omega_p = 5.5$ s. The left end of the circuit is connected to an oscillating voltage source $\Phi_I = A_0\cos(\varphi - \omega_0 t)$, where $A_0 = 14$ V, and the right end is measured by an oscilloscope to obtain Φ_T for the forward case, while for the backward case, the positions of Φ_I and Φ_T are switched (Supplemental Material 5 [28]).

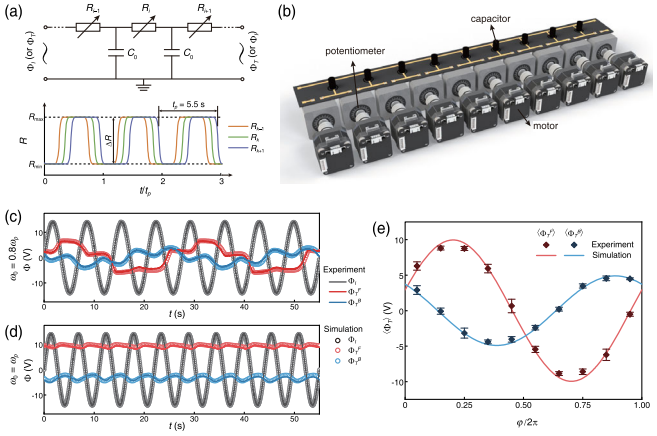

FIG. 4. Experimental verification of nonreciprocal voltage transmission under spatiotemporal modulation. (a) Equivalent circuit model for a medium with spatiotemporally modulated conductivity, consisting of a series of time-varying resistors alternated by fixed capacitors. (b) The system built according to the equivalent circuit in (a). 10 rotary potentiometers are driven by 10 mechanical motors to produce spatiotemporally varying resistance distributions. (c)–(d) Experimentally measured voltage when the frequencies of Φ_I are taken as $\omega_0 = 0.8\omega_p$ (c) and $\omega_0 = \omega_p$ (d). The lines are experimental results and the scatter points refer to simulated results using the same setup as the experiment. (e) Experimental results of the dependence of the drag effect (characterized by the time-averaged voltage) on the initial phase φ.

First, we select $\varphi = \pi/2$ and choose different ω_0 to obtain the performance of Φ_T. We give the measurement results for the cases $\omega_0/\omega_p = 0.8$ and 1 in Figs. 4(c) and 4(d). Moreover, results of more cases ($\omega_0/\omega_p = 0.2$, 1.1 and 2) are summarized in Fig. S4 [28]. Obviously, a voltage bias occurs in the coupled case. Next, we restrict the frequency of Φ_I at $\omega_0 = \omega_p$ and observe the dependence of the voltage bias on the initial phase φ of the input source. (See Supplemental Material, movie 1 for the evolution with time by tuning ω_0 and φ.) It can be seen that the voltage bias varies over a wide range with respect to φ in Fig. 4(e), where the bias is calculated by averaging the voltage over 10 modulation periods after reaching the quasisteady state. For reference, we also present the finite element numerical results using the circuit module of COMSOL Multiphysics®, in which the parameter setting is the same as the experiment. Despite the errors from the unstable motor frequency, inaccurate initial phase, etc., the experiment has proven the phenomena predicted by our theory. Apart from the aforementioned circuit, compressible composites [32,33] may also be good experimental candidates for producing a spatiotemporally varied conductivity. Although the proposed experimental setup is in the field of charge diffusion, the equivalent circuit is also suitable for verifying the transport of heat and mass. Their counterparts can be realized by using materials with

variable thermal conductivity or diffusivity and applying an oscillating heat or material source.

In summary, we have theoretically and experimentally reported the nonreciprocal transport of diffusion waves through spatiotemporally modulated systems. The space-time mode transitions to zero frequency account for the drag phenomenon of the transmission potential. It should be added that the occurrence of drag is not confined to the above setting of boundary conditions. For example, if we apply an oscillating potential at one port and a constant potential at the other, there will exist a flux drag, i.e., a dc flow [34], through the system (Supplemental Material 6 and Figs. S5-S7 [28]). We observe the asymmetric time-averaged flux in the coupled cases, whose rectification ratios are dependent on the modulation parameters such as Δ_σ, v_p, and φ.

The conclusion may be also extended to other diffusion-wave fields like carrier-density waves in electronic media (notably semiconductors), thermal waves, chemical waves and diffuse-photon-density waves [35–37], for their governing equations are same or similar to the formalism mentioned in this Letter. Especially in thermal and mass diffusion, since the two-parameter (conductivity and capacity) modulation [17,38] is extremely difficult to implement practically, the approach proposed here may provide feasible ways to generate nonreciprocity or design new-type diodes. For instance, it is possible to design thermal metamaterials [39–46] whose output end is heated or cooled in the forward or backward case (See Supplemental Material, movie 2 for the temperature evolution with time). This approach may also find applications in controlling signal transmission and information communication [47,48], such as filtering, rectification, etc.

C.-W. Q. acknowledges the support from Ministry of Education, Singapore (Grant No.: A-8000107-01-00). T. L. acknowledges the support of the National Key Research and Development Program (Grant No. 2022YFB4701700) and the National Natural Science Foundation of China (Grant No. 52175009).

*These authors contributed equally to this work.
†tianlongli@hit.edu.cn
‡chengwei.qiu@nus.edu.sg

[1] A. Mandelis, *Diffusion Wave Fields: Green Functions and Mathematical Methods* (Springer Science & Business Media, New York, 2001).
[2] A. Mandelis, Phys. Today **53**, No. 8, 29 (2000).
[3] M. Farhat, P. Y. Chen, H. Bagci, C. Amra, S. Guenneau, and A. Alu, Sci. Rep. **5**, 9876 (2015).
[4] L. J. Xu and J. P. Huang, Int. J. Heat Mass Transfer **159**, 120133 (2020).
[5] Z. Zhang, L. Xu, and J. Huang, Adv. Theory Simul. **5**, 2100375 (2021).
[6] R. J. Potton, Rep. Prog. Phys. **67**, 717 (2004).
[7] Y. Li, J. Li, M. Qi, C.-W. Qiu, and H. Chen, Phys. Rev. B **103**, 014307 (2021).
[8] L. Tang, J. Tang, M. Chen, F. Nori, M. Xiao, and K. Xia, Phys. Rev. Lett. **128**, 083604 (2022).
[9] D. L. Sounas and A. Alu, Nat. Photonics **11**, 774 (2017).
[10] A. M. Shaltout, V. M. Shalaev, and M. L. Brongersma, Science **364**, eaat3100 (2019).
[11] L. Zhang, X. Q. Chen, R. W. Shao, J. Y. Dai, Q. Cheng, G. Castaldi, V. Galdi, and T. J. Cui, Adv. Mater. **31**, 1904069 (2019).
[12] J. Li, C. Shen, X. Zhu, Y. Xie, and S. A. Cummer, Phys. Rev. B **99**, 144311 (2019).
[13] X. Wen, X. Zhu, A. Fan, W. Y. Tam, J. Zhu, H. W. Wu, F. Lemoult, M. Fink, and J. Li, Commun. Phys. **5**, 18 (2022).
[14] Zhaoxian Chen, Yugui Peng, Haoxiang Li, Jingjing Liu, Yujiang Ding, Bin Liang, Xue-Feng Zhu, Yanqing Lu, Jianchun Cheng, and Andrea Alù, Sci. Adv. **7**, eabj1198 (2021).
[15] G. Trainiti and M. Ruzzene, New J. Phys. **18**, 083047 (2016).
[16] H. Nassar, H. Chen, A. Norris, M. Haberman, and G. Huang, Proc. R. Soc. A **473**, 20170188 (2017).
[17] D. Torrent, O. Poncelet, and J.-C. Batsale, Phys. Rev. Lett. **120**, 125501 (2018).
[18] M. Camacho, B. Edwards, and N. Engheta, Nat. Commun. **11**, 3733 (2020).
[19] Z. F. Yu and S. H. Fan, Nat. Photonics **3**, 91 (2009).
[20] Z. F. Yu and S. H. Fan, in *Nonlinear Photonics and Novel Optical Phenomena*, edited by Z. Chen and R. Morandotti (Springer New York, New York, NY, 2012), p. 343.
[21] H. Lira, Z. F. Yu, S. H. Fan, and M. Lipson, Phys. Rev. Lett. **109**, 033901 (2012).
[22] P. C. Kuan, C. Huang, W. S. Chan, S. Kosen, and S. Y. Lan, Nat. Commun. **7**, 13030 (2016).
[23] P. A. Huidobro, E. Galiffi, S. Guenneau, R. V. Craster, and J. B. Pendry, Proc. Natl. Acad. Sci. U.S.A. **116**, 24943 (2019).
[24] Y. Dong *et al.*, Nature (London) **594**, 513 (2021).
[25] W. Y. Zhao *et al.*, Nature (London) **594**, 517 (2021).
[26] L. Xu, G. Xu, J. Huang, and C.-W. Qiu, Phys. Rev. Lett. **128**, 145901 (2022).
[27] R. Cheng, F. Wang, L. Yin, Z. Wang, Y. Wen, T. A. Shifa, and J. He, National electronics review **1**, 356 (2018).
[28] See Supplemental Material at http://link.aps.org/supplemental/10.1103/PhysRevLett.129.256601 for details on the dispersion relation (Note 1), the explicit dispersion relation for the limit of $\Delta_\sigma \to 0$ (Note 2), the analysis of the special cases of $\beta_p = 0$ or $\omega_p = 0$ (Note 3), the analytical solution of the diffusion equation under spatiotemporal modulation (Note 4), the setups of our experimental platform (Note 5), the flux transmission under spatiotemporal modulation (Note 6), and supplemental figures and movies.
[29] E. S. Cassedy and A. A. Oliner, Proc. IEEE **51**, 1342 (1963).
[30] S. Taravati, Phys. Rev. Appl. **9**, 064012 (2018).
[31] A. T. Forrester, R. A. Gudmundsen, and P. O. Johnson, Phys. Rev. **99**, 1691 (1955).
[32] Chaoji Chen, Jianwei Song, Jian Cheng, Zhenqian Pang, Wentao Gan, Gegu Chen, Yudi Kuang, Hao Huang,

Upamanyu Ray, Teng Li, and Liangbing Hu, ACS Nano **14**, 16723 (2020).
[33] T. Du, Z. Xiong, L. Delgado, W. Liao, J. Peoples, R. Kantharaj, P. R. Chowdhury, A. Marconnet, and X. Ruan, Nat. Commun. **12**, 4915 (2021).
[34] T. J. Shimokusu, Q. Zhu, N. Rivera, and G. Wehmeyer, Int. J. Heat Mass Transfer **182**, 122035 (2022).
[35] M. Farhat, S. Guenneau, T. Puvirajesinghe, and F. H. Alharbi, Opt. Express **26**, 24792 (2018).
[36] R. Schittny, A. Niemeyer, M. Kadic, T. Buckmann, A. Naber, and M. Wegener, Opt. Lett. **40**, 4202 (2015).
[37] R. Schittny, A. Niemeyer, M. Kadic, T. Buckmann, A. Naber, and M. Wegener, Optica **2**, 84 (2015).
[38] Jiaxin Li, Ying Li, Pei-Chao Cao, Minghong Qi, Xu Zheng, Yu-Gui Peng, Baowen Li, Xue-Feng Zhu, Andrea Alù, Hongsheng Chen, and Cheng-Wei Qiu, Nat. Commun. **13**, 167 (2022).
[39] Y. Li, X. Bai, T. Z. Yang, H. L. Luo, and C. W. Qiu, Nat. Commun. **9**, 273 (2018).
[40] Ying Li, Ke-Jia Zhu, Yu-Gui Peng, Wei Li, Tianzhi Yang, He-Xiu Xu, Hong Chen, Xue-Feng Zhu, Shanhui Fan, and C.-W. Qiu, Nat. Mater. **18**, 48 (2019).
[41] Y. Li, W. Li, T. Han, X. Zheng, J. Li, B. Li, S. Fan, and C.-W. Qiu, Nat. Rev. Mater. **6**, 488 (2021).
[42] J. Li, Y. Li, T. Li, W. Wang, L. Li, and C.-W. Qiu, Phys. Rev. Appl. **11**, 044021 (2019).
[43] J. Li, Y. Li, W. Wang, L. Li, and C.-W. Qiu, Opt. Express **28**, 25894 (2020).
[44] J. Li, Y. Li, P.-C. Cao, T. Yang, X.-F. Zhu, W. Wang, and C.-W. Qiu, Adv. Mater. **32**, 2003823 (2020).
[45] G. Xu, Y. Li, W. Li, S. Fan, and C.-W. Qiu, Phys. Rev. Lett. **127**, 105901 (2021).
[46] G. Xu, Y. Yang, X. Zhou, H. Chen, A. Alù, and C.-W. Qiu, Nat. Phys. **18**, 450 (2022).
[47] Z. Chen and M. Segev, eLight **1**, 2 (2021).
[48] Y. Luo, Y. Zhao, J. Li, E. Çetintaş, Y. Rivenson, M. Jarrahi, and A. Ozcan, eLight **2**, 4 (2022).